Journal Pre-proof

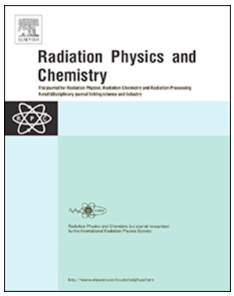

Crosslinked networks in electron beam irradiated polyethylenes evaluated by proton low-field NMR spectroscopy

Pilar Posadas, Juan L. Valentín, Rosario Benavente, Enrique Blázquez-Blázquez, Ane Urtiaga, Juan A. Álvarez, María L. Cerrada

PII: S0969-806X(22)00757-5

DOI: https://doi.org/10.1016/j.radphyschem.2022.110694

Reference: RPC 110694

To appear in: *Radiation Physics and Chemistry*

Received Date: 5 October 2022

Revised Date: 30 November 2022

Accepted Date: 30 November 2022

Please cite this article as: Posadas, P., Valentín, J.L., Benavente, R., Blázquez-Blázquez, E., Urtiaga, A., Álvarez, J.A., Cerrada, Marí.L., Crosslinked networks in electron beam irradiated polyethylenes evaluated by proton low-field NMR spectroscopy, *Radiation Physics and Chemistry* (2023), doi: https://doi.org/10.1016/j.radphyschem.2022.110694.

Author statement

Pilar Posadas: Conceptualization, Methodology, Investigation, Writing - Original Draft, Writing - review & editing. **Juan L. Valentín**: Conceptualization, Methodology, Investigation, Writing - review & editing. **Rosario Benavente**: Investigation, Writing - review & editing. **Enrique Blázquez-Blázquez**: Investigation, Writing - review & editing. **Ane Urtiaga**: Investigation, Writing - review & editing. **Juan A. Álvarez**: Investigation, Writing - review & editing. **María L. Cerrada**: Methodology, Investigation, Writing - Original Draft, Writing - review & editing.

CROSSLINKED NETWORKS IN ELECTRON BEAM IRRADIATED POLYETHYLENES EVALUATED BY PROTON LOW-FIELD NMR SPECTROSCOPY

Pilar Posadas[a*], Juan L. Valentín[a], Rosario Benavente[a], Enrique Blázquez-Blázquez[a], Ane Urtiaga[b], Juan A. Álvarez[c], María L. Cerrada[a*]

[a]Instituto de Ciencia y Tecnología de Polímeros (ICTP-CSIC). C/ Juan de la Cierva, 3, 28006 Madrid, Spain.

[b]Departamento de Ingenierías Química y Biomolecular. Universidad de Cantabria. Avda. Los Castros 46, 39005 Santander, Spain.

[c]Departamento de I+D, Calidad y Medio Ambiente. Grupo Armando Álvarez. Avda. Pablo Garnica 20, 39300 Torrelavega (Cantabria), Spain.

*E-mail addresses of corresponding authors:

pposadas@ictp.csic.es (P. Posadas); mlcerrada@ictp.csic.es (M. L. Cerrada)

Abstract

Effect of electron beam (EB) irradiation is analyzed in low and high density polyethylenes (LDPE and HDPE, respectively) at different doses. Parameters as important as degree of crystallinity, melting or crystallization temperatures are dependent on the initial PE molecular architecture, which also controls the gel content developed by action of EB irradiation and the EB dose applied. Thus, this gel amount, ascribed to formation of chain crosslinkings, is raised as irradiation dose increases, being larger in the HDPE than in the LDPE. In both, a plateau value is reached at the highest doses. The molecular changes that take place in both PEs during EB irradiation lead to a hindrance in their crystallization capacity, once macrochains are molten, and, accordingly, to a reduction in crystallinity and to formation of thinner crystallites. Variation with temperature of rigid and soft fractions together with their respective relaxation times is followed in the irradiated LDPE and HDPE specimens by pulse mixed magic-sandwich echo nuclear magnetic resonance (MSE-NMR) measurements. The network structure promoted in these PEs is evaluated by using the multiple-quantum nuclear magnetic resonance (MQ-NMR) approach, showing important differences caused by EB irradiation due to their intrinsic molecular characteristics.

Keywords: LDPE and HDPE, crystallinity, Low field NMR, rigid and soft phases, crosslink density, network structure.

Introduction

Polyethylene (PE) is a thermoplastic polymer that consists of long-range chains of hydrocarbons. Nowadays, PE plays a key position in the manufacture of plastics for uses in agriculture, packaging and medical devices[1], among other application fields. There are three main types of PE: high density (HDPE), low density (LDPE) and linear low density (LLDPE). Each class shows different characteristics. Hence, HDPE provides barrier properties, chemical resistance and stiffness while LDPE offers an excellent impact response and resistance to stress cracking[2]. The use of PE is, however, restricted in certain applications because of its low melting temperature, its solubility or swelling in hydrocarbons and its trend to crack when subjected to stresses. Different processes have been employed to optimize and maximize its final performance. A significant work on crosslinking of PE was done in the late 1950s, finding that PE properties could be enhanced by means of chemical crosslinking through irradiation[3]. Irradiated crosslinked PE was the starting point for many jacketing compounds in cables and wires as well as for tubing and heat-shrinkable films. Crosslinked PE shows an enlarged dimensional stability during its exposure to heat due to the formation of a three-dimensional network. This network also provides a higher resistance towards stress cracking and chemicals leading to a more durable material[2,4].

Electron beam (EB) irradiation by means of accelerated electrons is currently the most used approach. Upon irradiation, some chemical changes are boosted in the PE[4,5], all of them including formation of free radicals: recombination and chain branching, scission of bonds, crosslinking of chains and different oxidation reactions (in presence of air). The dose applied, the environment surrounding during radiation, the post-irradiation treatment, the initial molecular weight and other molecular characteristics have been described to affect the extent of these mechanisms[6–10], since all of these numerous and simultaneous irradiation-induced defects compete between them. Nevertheless, PE primarily undergoes crosslinking in the amorphous regions or at the boundaries of crystallites[2,4] at intermediate and high doses. Thus, EB irradiation provides an easy protocol to induce this crosslinking in PEs through a manufacturing process that implies short times and it is performed at room temperature and under normal pressure.

A thorough knowledge of these changes in the PE structure requires a quantitative characterization of phases composition and of molecular mobility[11]. In this sense, solid-state NMR is a powerful tool to study polymer networks[12–20]. On one hand,

multiple-quantum nuclear magnetic resonance (MQ-NMR) method allows the direct access to residual dipolar coupling constants that persist because of the existence of cross-links and other topological constrains[15,16,19–21]. This experimental procedure is, therefore, an effective means for quantifying the microstructure[17] in addition to evaluate the dynamics of polymeric chain[11], providing a complete picture of the network structure. On the other hand, pulsed mixed magic-sandwich echo (MSE) method offers a near-quantitative refocusing of the rigid contribution to the initial part of the free induction decay (FID)[15,19,22], which supplies an essentially quantitative determination of phases composition of these complex polymer structures.

The aim of this work is, therefore, to study the effect that EB irradiation provokes in the structure and phases composition of two rather different polyethylenes: a low density LDPE and a high density HDPE. Accordingly, different doses of ionizing EB irradiation were applied on PE films at room temperature. Then, gel content, which is mainly related to formation of chain crosslinkings, and location of the thermal transitions were determined for these PEs. Furthermore, a comprehensive analysis of the network structure was performed by low-field NMR. An isotactic polypropylene, iPP, was also analyzed for a better understanding of some of the results.

Experimental part

Materials

Two types of polyethylene (PE), both supplied by Repsol, have been analyzed: a low density grade, named as LDPE, with a density of 0.9280 g/cm^3; and, a high-density one, referred as HDPE with a density[2] of 0.9499 g/cm^3.

A commercially available metallocene isotactic polypropylene, labeled as iPP, with trade name of Purell HM671T, kindly supplied by Basell, has been also used in the present research[6]. Its density was 0.90 g/cm^3.

Preparation of films

Multilayer LDPE films, with five layers of identical PE composition, were obtained by extrusion-blowing in a machine Extrusion Lab GAA 5 layers.

Compression molded HDPE and iPP films were prepared in a Collin press between hot plates at 170º and 190 ºC, respectively, at a pressure of 1.5 MPa for 4 min. A fast cooling from the melt was applied between plates of the press refrigerated with cold water, at an approximate rate of 80 ºC/min. Thickness for all of these films is around 100 μm.

Irradiation of specimens

EB irradiation was carried out at IONMED (an industrial installation) in atmospheric air at ambient temperature using a 10 MeV Rhodotron accelerator. All polymeric films were irradiated using a current of 5 mA. Several passes under these conditions were required for changing irradiation doses, which are reported in Table 1 for the different polymers.

Table 1.EB irradiation doses used in the different polymers analyzed.

Polymer	EB irradiation doses (kGy)
LDPE	27, 83, 109, 137, 193, 221
HDPE	33, 67, 133, 233
iPP	34, 67, 134, 235

The different specimens were labeled as LDPE_*x* or HDPE_*x*, where *x* refers to the EB dose applied (kGy). Non-irradiated samples were simply designated as LDPE and HDPE, respectively.

Gel content determination

The gel content (insoluble fraction) of the various specimens was determined gravimetrically, according to ASTM D 2765, using a 16 h Soxhlet extraction cycle, with *p*-xylene as solvent, at 140ºC. The polymeric samples were cut into small pieces and placed in a pre-weighed stainless steel fine wire mesh. After the extraction cycle, samples were washed with acetone and vacuum-dried to constant weight. The gel content was calculated as the percentage ratio of the final weight of the insoluble polymeric fraction to its initial weight prior to extraction.

Differential scanning calorimetry

Calorimetric analyses were carried out using a Perkin Elmer DSC 7 calorimeter, connected to a cooling system and calibrated with various standards. The sample weights ranged from 6 to 8 mg. A temperature interval from -50 to 180 ºC was studied and the different runs were carried out at a heating rate of 10 ºC/min. For crystallinity determination, a value of 290 J/g was taken as the enthalpy of fusion of perfectly crystalline material for PE[23,24]and 165 J/g for iPP[25,26].

^{1}H-NMR experiments

Time-domain ^{1}H NMR experiments were performed on a low-field Bruker Minispec mq20 spectrometer at 20 MHz proton resonance frequency, operating at 0.5 T, with 90º pulses of 3.1 µs length and a dead time of 12 µs. The sample temperature was

controlled with a BVT3000 heater working with air. In order to avoid degradation, samples were flamed-sealed in 8 mm NMR tubes under vacuum conditions. Two approaches: magic sandwich echo (MSE) and double-quantum (DQ) experiments were used for characterizing the complex structure of these materials. On one hand, the former is useful for determination of mobility in the different fractions present in these polymers and their dependence on temperature. In this sense, MSE measurements were carried out from 40 to 140ºC. On the other hand, DQ experiments provide information about the restriction of chains mobility as a consequence of entanglements and crosslinks. Measurements were performed at 150 º and 180 ºC.

Results and discussion

Gel content and phase transitions

Figure 1 shows the gel content determined for the LDPE and HDPE in the interval of irradiation doses used. A zero gel amount is observed in the non-irradiated samples[2], fact that indicates that the whole sample is completely soluble in *p*-xylene at 140 ºC or that density of the crosslinks formed, in relation to other defects, is not sufficient to induce the formation of a gel fraction. Obtainment of a small fraction of crosslinked chains, which is associated with the development of an insoluble gel, is noted at around 30 kGy, either for the LDPE or the HDPE specimens. The little amount of free radicals developed at this low dose leads, in majority, to scission or branching within chains. This gel content increases as irradiation dose does, although the rise is in HDPE greater than in LDPE. Therefore, it could be said looking at Figure 1 that crosslinking is not preferentially favored at doses smaller than 100 kGy, although the formation of a network in the amorphous regions is boosted at higher doses in a larger extent in HDPE than in LDPE.

Differences between HDPE and LDPE can be associated with the specific molecular details existing in their architectures, since branching content is much larger in LDPE than in HPDE. These branches imply presence of larger amounts of tertiary carbons in the LDPE macrochains that promote other mechanisms (scission, branching or oxidation) different to crosslinking by the action of EB irradiation. Accordingly, gel content, which is associated with the crosslinked fraction within the amorphous phase, is in LDPE lower than that in the highly crosslinkable HDPE. Importance of presence in tertiary carbons for preventing chemical network formation has been described in literature[27] and it was also deduced from soxhlet extraction results achieved in iPP samples that revealed total solubility in *p*-xylene at 140 ºC in the different specimens

analyzed, independently of the dose applied. Thus, EB irradiation did not trigger development of crosslinks between iPP macrochains within the dose range analyzed, or their density, relative to other defects, was not enough to induce the formation of a gel fraction. The mechanisms described for iPP after its exposure to EB radiation are mainly scission, branching and oxidation, when it is irradiated under an oxygen atmosphere, but not formation of crosslinks[6]. Content of tertiary carbons within the iPP architecture is much higher than in LDPE and a full hindrance of crosslinks development is achieved within this range of EB doses.

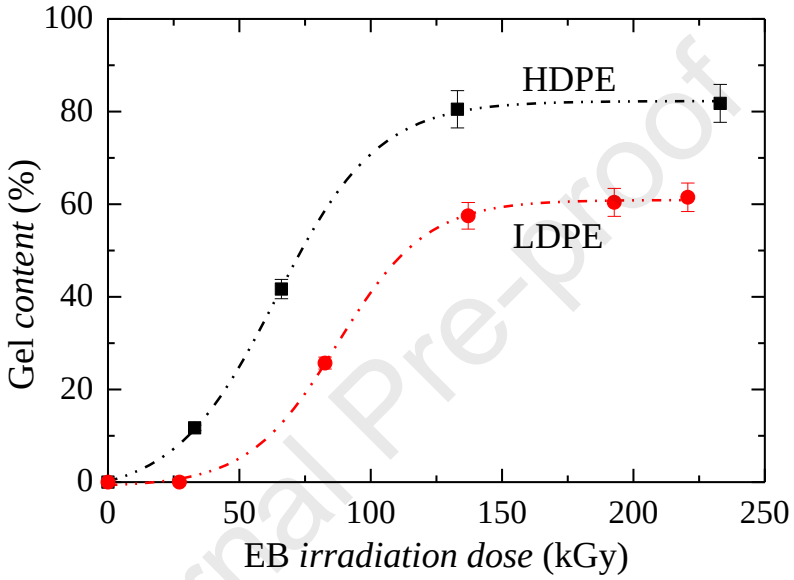

Figure 1. Effect of the irradiation doses on the gel content of the samples LDPE and HDPE.

Figure 2 shows the phase transitions found in the crystalline regions of the non-irradiated LDPE and HDPE specimens together with those observed in some of the irradiated samples. Effect of molecular architecture is clearly evident between LDPE and HDPE by comparison of these figures. Presence of branches in LDPE macrochains breaks its regularity and, thus, its crystallization capability is reduced compared with that existing in the linear HDPE macromolecules. These features imply lower degree of crystallinity and smaller crystals in LDPE than in HDPE. Accordingly, crystallinity is around 0.64 for HDPE and 0.52 for LDPE while melting temperature (T_m) is 133 ºC in the former and 115 ºC in the latest. Crystallization temperature (T_c) is also affected, appearing at 112 ºC for the HDPE and at around 105 ºC in LDPE. As aforementioned, these distinct characteristics are ascribed to their molecular differences.

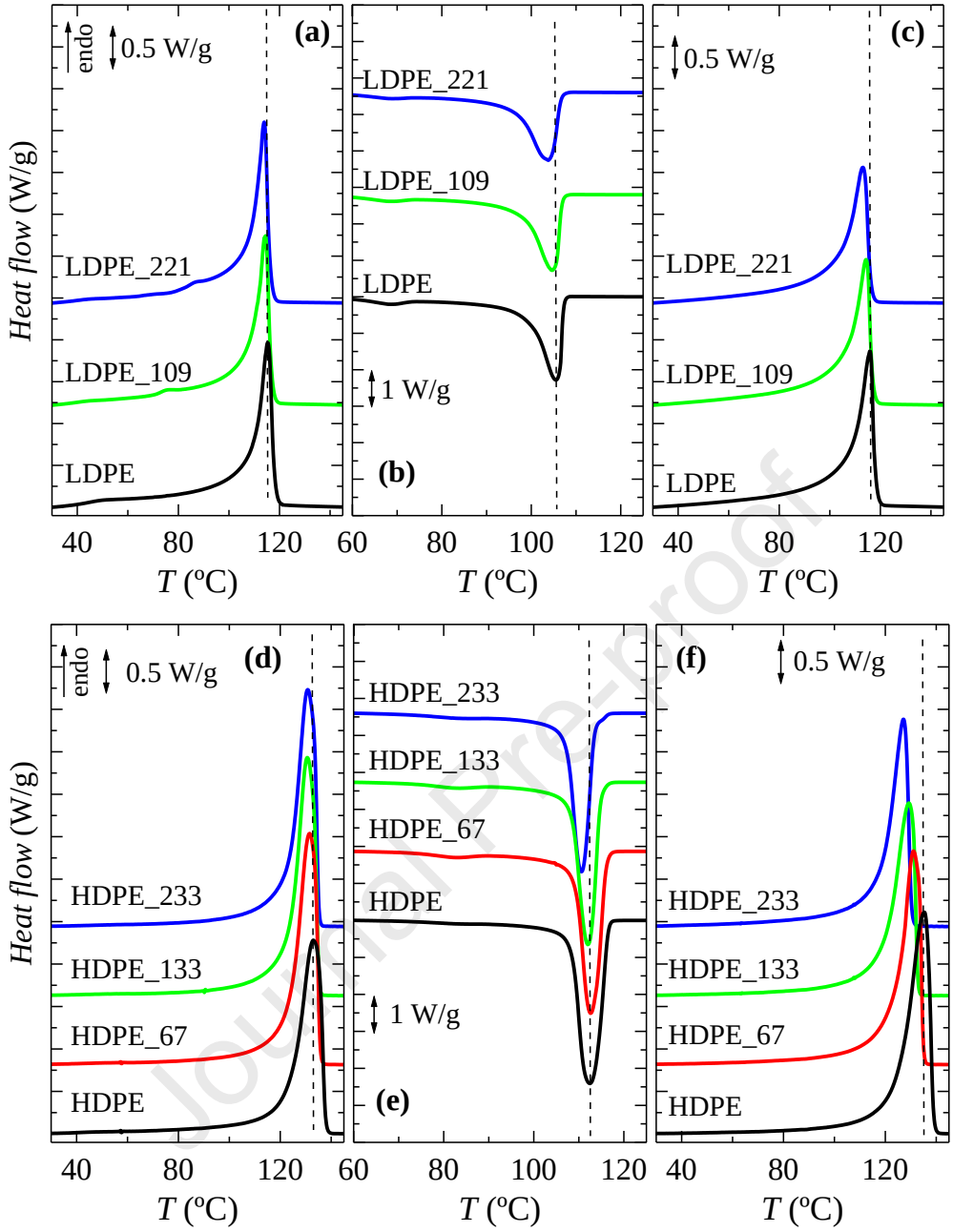

Figure 2. Phase transitions found in the crystalline regions of either pristine or irradiated LDPE and HDPE specimens obtained by DSC experiments performed at a scanning rate of 10 °C/min: (a and d) first melting; (b and e) crystallization; and, (c and f) subsequent melting after crystallization at 10 °C/min.

The global effect of EB irradiation in the thermal transitions is, however, rather similar for these two types of PEs. A slight displacement of T_m to lower temperature is observed with irradiation dose along the first melting process after irradiation at room temperature: from 115.5 ºC to 114 ºC between the non-irradiated LDPE and the LDPE_221, respectively; and, from 133 ºC to 131 ºC between the pristine HDPE and the irradiated HDPE_233. Furthermore, degree of crystallinity remains unchanged

during the first heating experiment (see Table 2). Irradiation leads, above a specific dose, to formation of crosslinks between the chains located in the amorphous regions, in more extent in the HDPE than in LDPE, as deduced from its higher gel content values. This process competes with other simultaneous mechanisms induced by the free radicals produced, but crystallites, which were developed in a previous stage during film processing, are practically unaffected.

Table 2. Degree of crystallinity determined by DSC estimated from the first and second heating runs (f_c^{m1}, and f_c^{m2}, respectively)

sample	f_c^{m1}	f_c^{m2}	sample	f_c^{m1}	f_c^{m2}
HDPE_0	0.64	0.67	LDPE_0	0.52	0.50
HDPE_33	0.64	0.66	LDPE_27	0.52	0.50
HDPE_67	0.64	0.65	LDPE_83	0.52	0.50
			LDPE_109	0.52	0.49
HDPE_133	0.64	0.62	LDPE_137	0.52	0.49
			LDPE_193	0.52	0.49
HDPE_233	0.64	0.62	LDPE_221	0.52	0.49

Once the polymer is completely molten, this isotropic state is, however, different from the initial one, from where films were manufactured, because of the formation of amorphous chain networks in the amorphous regions during EB irradiation. In addition, this molten state is now also dependent on the irradiation dose. Thus, it is very interesting and mandatory to analyze how the PE crystallization is affected by EB irradiation as well as the subsequent melting process. Concerning the former, location of T_c does not change much, going down from 105.5 ºC to 103.5 ºC, respectively for the neat LDPE and for LDPE_200, while it appears at 112 ºC in the pristine HPDE and at 111 ºC for the irradiated HDPE_233. Nevertheless, degree of crystallinity is reduced, more significantly in HDPE than in LDPE samples, being the values analogous to those defined as f_c^{m2} in Table 2. This feature can be ascribed to the hindrance imposed by the crosslinked and the branched chains within this new molten state existing after solid state irradiation.

This decrease in crystallinity as well as the development of thinner crystallites is also noticeable in the second heating run where the area under melting curve is diminished and the T_m is shifted to lower temperatures as dose is increased. This effect

has been analyzed in detail in the literature[28] . In the samples under analysis, the influence is more remarkable in the HDPE than in LDPE because the amount of crosslinks at the highest doses is larger in the former, as deduced from the gel content related to the initial chains located in the amorphous regions, as aforementioned. Therefore, variations in LDPE are from 0.50 to 0.49 for the crystallinity and from 116 ºC to 113 ºC for the T_m between the neat and that subjected to a dose of 221 kGy whereas differences are in the HDPE: 0.67 and 0.62 for degree of crystallinity and 134 ºC and 127 ºC for T_m between the pristine specimen and that subjected to a dose of 233 kGy[29].

Quantitative phase composition and evolution of different phases with the temperature

PE is a semicrystalline polymer. Accordingly, it is composed of domains with widely different chain mobility. Chains are highly ordered in the crystalline domain and can reorient only very slowly[30]. PE crystallizes in an orthorhombic lattice under the common processing conditions[31] and its crystallites have usually a lamellar morphology. Only methyl branches can be included in the crystalline cell to a substantial degree[32–36] and a small proportion of ethyl ones has been also found in crystalline environments[37,38]. The excluded branches form an interfacial region that is more ordered than the amorphous one[39].The PE chains in the non-crystalline domains are the most mobile. Degree of chains mobility in the interlamellar non-crystalline regions depends on the distance to lamellar crystalline surfaces in such a way that the chains next to crystals are somewhat ordered and only moderately mobile while those that are further away from crystals are amorphous[30].

A quantitative characterization of the phases composition and the molecular mobility has a huge importance[11]. The former is probably one of the most important morphological parameters, mainly because the amorphous and crystalline phases exhibit vastly different behavior and their relative contributions to the material properties should be accurately known[2,11,30,40].

Solid-state NMR is a useful method for characterizing phase composition in these systems. The rigid fraction usually decays in the first 20 μs of the free-induction decay, thus the signal detected after the dead time (<12 μs in the case of the used spectrometer) partially conceals this information, which is a key issue in order to quantify the fraction of protons in rigid environments with restricted mobility. In this

sense, pulse mixed magic-sandwich echo (MSE-NMR) measurements are a robust method to investigate polymer mobility[22,41,42]. They were performed using a pulse sequence detailed elsewhere[22,41,42] at different temperatures from 40 º to 140 ºC. Therefore, MSE-FID curves were employed to quantify the rigid and soft fractions in PE samples. The first fast decay is ascribed to the rigid polymer fraction in the MSE-FID whereas the slower signal decay is assigned to a soft fraction. Hence, the first 140 μs of the normalized MSE-FID curves (unity signal for zero time) were fitted according to equation 1:

$$I_{MSE-FID} = A \exp\left[-\left(\frac{\tau}{T_{2rigid}}\right)\right]^{n_1} + (1-A)\exp\left[-\left(\frac{\tau}{T_{2soft}}\right)\right]^{n_2} \quad (1)$$

In this expression, A is the fraction of detectable rigid phase in the sample and n_1 and n_2 are two adjustable parameters for a better fit of the fast decay shape.

At temperatures well above glass transition (T_g), which is characteristic of the amorphous phase, the T_2-relaxation decay for PE can be usually decomposed into three components, which come from the crystalline phase, from a semi-rigid crystal-amorphous interface and from the soft fraction involved in amorphous phase. The intermediate one has distinct dynamic properties and may not be considered as a true thermo-dynamic phase. Apparently, the definition of an interface or a semi-rigid fraction of the amorphous phase is more appropriate for this phase[11]. Taking into account this fact, MSE-FIDs were fitted according the following expression:

$$I_{MSE-FID} = A \exp\left[-\left(\frac{\tau}{T_{2rigid}}\right)\right]^{n_1} + B \exp\left[-\left(\frac{\tau}{T_{2interface}}\right)\right]^{n_2} + (1-A-B)\exp\left[-\left(\frac{\tau}{T_{2soft}}\right)\right]^{n_3} \quad (2)$$

In equation 2, B is the detectable fraction of semi-rigid phase in the sample. In all cases, $n_1 \approx 2$ (*i.e.*, the crystalline fraction is described by a Gaussian function) and n_3 remains constant and equal to n_2 of the equation 1. The rigid, semi-rigid and soft fractions, as well as n_2 and T_2 were calculated by using the equation 2 at different temperatures.

First of all, two phases are considered, rigid and soft fractions, because a two-phase model is traditionally[11] used to describe morphology in non-deformable melt-crystallized PE as well as in other semicrystalline polymers. As mentioned, MSE-NMR

method is based on decomposition of the FID signal into components assigned to phases with different mobility[41,42]. Figure 3a shows the rigid and soft fractions, calculated from the normalized MSE-FID curves according to equation 1, in the raw LDPE polymer together with those achieved at the irradiation doses of 109 and 221 kGy, *i.e.*, LDPE_109 and LDPE_221. In Figure 3b, evolution of the T_2 transverse relaxation time with the temperature is shown for these rigid and soft fractions.

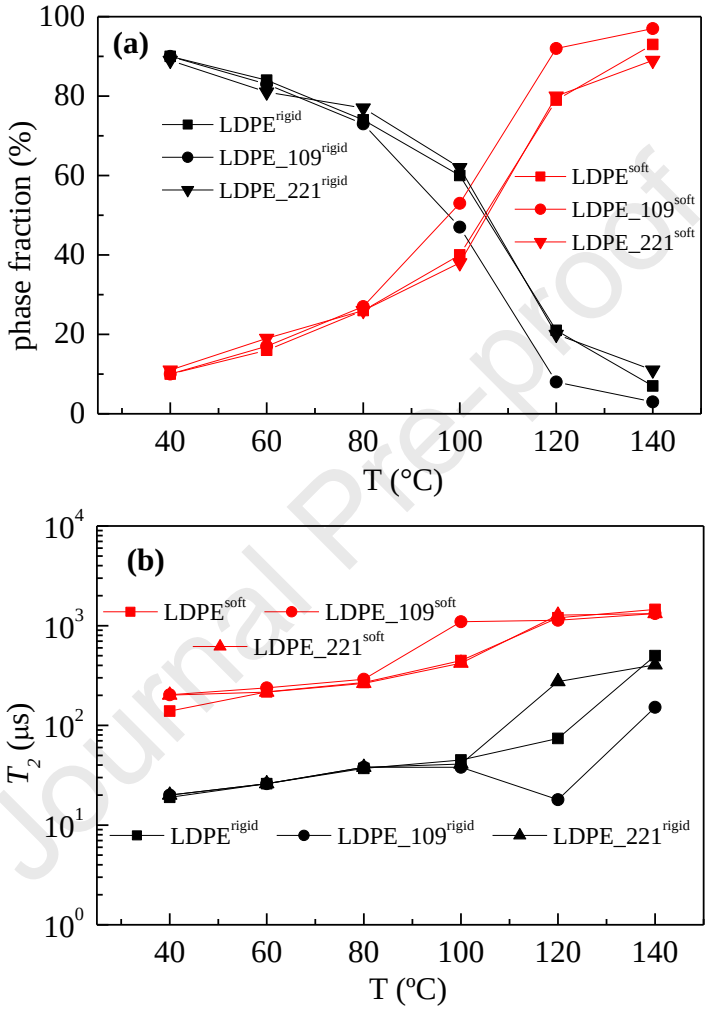

Figure 3. (a) Variation of the rigid and soft polymer fractions, deduced from MSE-FID curves as a function of the temperature, for neat and irradiated LDPE. (b) Temperature dependence of the T_2 relaxation times components: T_2^r (black symbols) and T_2^s (red symbols), which are assigned to the rigid and soft fractions, respectively.

Results of Figure 3a indicate that the rigid fraction is around 90% at 40 °C for all the LDPE specimens. As temperature increases, a continuous drop of the detected rigid phase proportion is observed until 100 °C temperature where an abrupt fall is noted. Finally, the rigid polymer phase proportion is near zero at 140 °C. These results are qualitatively consistent with those attained from DSC experiments for the first melting, although the amount of crystallites, which are the rigid components, determined by

DSC is around 52% and not 90%. The continuous decrease up to 100 °C corresponds to the loss with temperature of that rigid fraction since crystals of smallest size can start to melt from 40 °C because LDPE contains in its architecture a high proportion of long side chains[43]. The main melting process takes place in the interval ranging from 100 ° to 120 ºC, as deduced from DSC curves represented in Figure 2. EB irradiation might incorporate some small differences in this rigid fraction since the changes (formation of crosslinkings, scission of chains, their oxidation and their branching) occurring in the amorphous regions may somehow reduce the mobility of polymeric chains.

On the other hand, samples increase slightly their temperature for a short time during the EB irradiation process at room temperature, fact that can affect to some extent the population and perfection of the thinner crystals. Thus, small melting peaks can be observed at temperatures lower than that for the primary process, as seen for LDPE in Figure 2.

Figure 3b clearly shows two different behaviors in relation to T_2 transverse relaxation times. At low temperature, relaxation times exhibited by the rigid phase are around few microseconds while the soft phase shows relaxation times around hundreds of microseconds. As temperature increases, rather linear trends in T_2 are observed until 100 ºC. At higher temperatures, dependence is not linear and varies with irradiation.

Figure 4 shows the rigid and soft fractions as well as the evolution of the transverse relaxation time (T_2) with temperature now for the pristine HDPE and its specimens subjected to irradiation doses of 67, 133 and 233 kGy. The rigid fraction reaches a value of around 85% at 40 °C in the case of the non-irradiated HDPE. As temperature increases, a progressive decrease is observed with temperature until 120 ºC in this rigid phase. Again, these results are qualitatively in agreement with those from DSC experiments where maximum melting temperatures from the first and second heating runs are 133 ºC and 134 ºC, respectively. In addition, these results agree with the values obtained by SAXS in the literature[2].

This rigid phase is somehow different in the irradiated HDPE specimens, increasing its proportion at a given temperature compared with that in the pristine polymer. Irradiation has promoted high degree of crosslinkings in the amorphous HDPE regions, mainly at the two highest doses, as deduced from Figure 1, and this amorphous network also contributes to raise the overall rigidity.

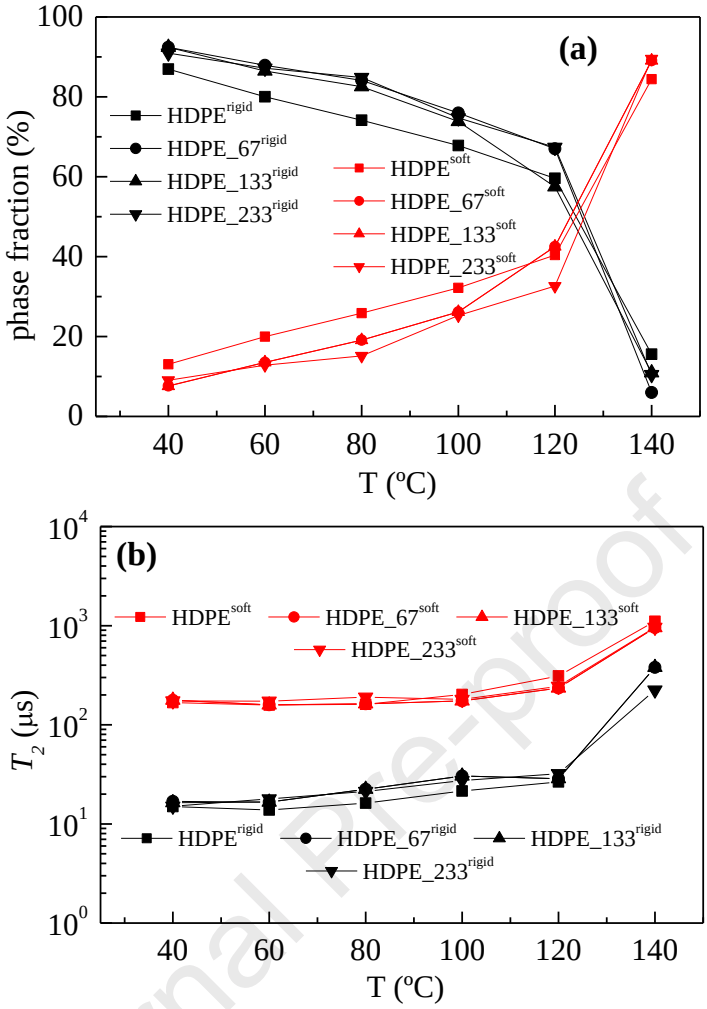

Figure 4. (a) Variation of the rigid and soft polymer fractions, deduced from MSE-FID curves as a function of the temperature, for neat and irradiated HDPE. (b) Temperature dependence of the T_2 relaxation times components: T_2^r (black symbols) and T_2^s (red symbols), which are assigned to the rigid and soft fractions, respectively.

Differences related to T_2 transverse relaxation times are also observed in HDPE, as already commented for LDPE: the rigid phase showing relaxation times about few microseconds while the soft component displays relaxation times around hundreds of microseconds at low temperatures. As temperature increases, a smooth almost linear dependence of T_2 upon temperature is observed until 120 ºC. At higher temperatures, a more remarkable increase is noticed.

As noted in LDPE, the values obtained in HDPE samples for the rigid component are also much higher than its degree of crystallinity. This remark can be associated with the fact that this model is too simple, taking into account that there is a fraction of polymer showing a gradient of mobility, starting at the rigid limit up to the core of the mobile phase, which is called interface or interphase, in the case of semicrystalline polymers as PE[11,41,44,45]. Contribution of this fraction seems to be rather

important[46] since without its consideration the rigid fraction obtained is as high as 90 % for the LDPE and 85 % for the HDPE, as aforementioned. For this reason, MSE has been decomposed into three components with different mobility, the rigid, T_2^r, the semi-rigid, T_2^{sr}, and the soft, T_2^s, fractions, respectively. Results achieved from application of this three-phase model are represented in Figure 5 for LDPE and in Figure 6 for HDPE.

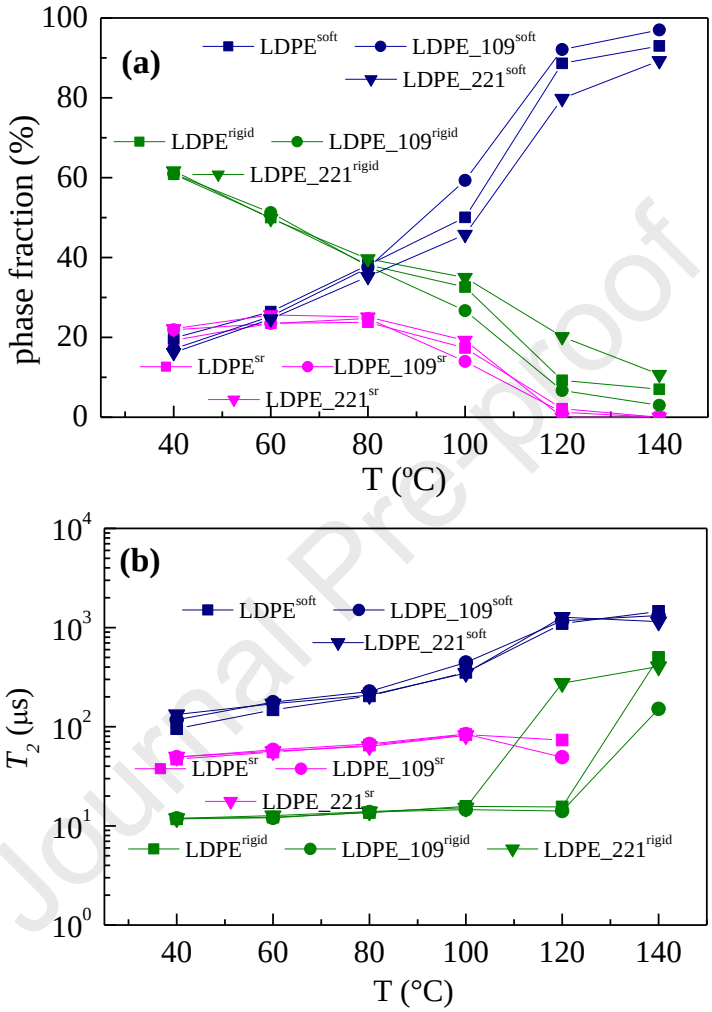

Figure 5. (a) Variation of the rigid, semi-rigid (sr) and soft polymer fractions, deduced from MSE-FID curves as a function of temperature, for neat and irradiated LDPE. (b) Temperature dependence of the T_2 relaxation time components: T_2^{rigid} (olive symbols), T_2^{sr} (magenta symbols) and T_2^{soft} (royal symbols), which are assigned to the rigid, semi-rigid (interphase) and soft, respectively.

Content in the rigid component is significantly reduced compared with that attained using a two-phase model, getting closer to the degree of crystallinity derived from DSC measurements for both PEs, although the rigid fraction estimated from MSE-FID curves is higher than crystallinity. As temperature increases, amount of the rigid component is progressively reduced as expected. The semi-rigid fraction is maintained almost constant up to 80 ºC in LDPE, temperature at which starts to decrease, while the

soft component raises its content along the whole temperature interval analyzed. Only soft polymeric phase remains at 140 °C.

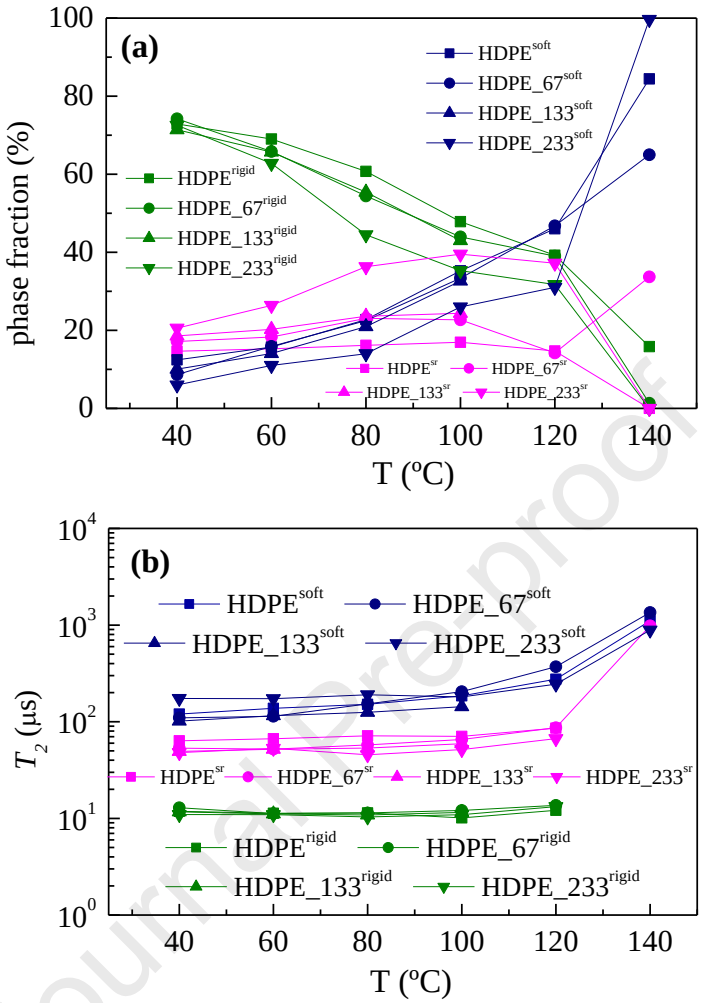

Figure 6. (a) Variation of the rigid, semi-rigid (sr) and soft polymer fractions, deduced from MSE-FID curves as a function of temperature, for neat and irradiated HDPE. (b) Temperature dependence of the T_2 relaxation time components: T_2^{rigid} (olive symbols), T_2^{sr} (magenta symbols) and T_2^{soft} (royal symbols), which are assigned to the rigid, semi-rigid (interphase) and soft, respectively.

In the neat HDPE, interphase fraction is close to the amorphous one at low temperatures. As it increases, the amount of semi-rigid fraction keeps under 20% while rising the amount of soft fraction and decreasing that for rigid fraction, due to the less constrained chain fragments in the amorphous phase and possibly by melting of thin lamellae that are inserted into the primary stack of crystallites[11]. This three phase model improves the description of the phase structure in HDPE, as showed in Figure 6a and 6b. At 140ºC, only soft phase remains in these four HDPE specimens studied in this work.

Network structure-properties relationships

Double-Quantum (DQ) NMR experiments were performed to determine the evolution of non-coupled network defects and the molecular weight between cross-links, M_c. Concerning the former, DQ NMR experiments allow quantifying the fraction of non-coupled defects as chain segments with isotropic motions that show slower relaxations from the polymer network, *i.e.*, segments that are dipolar coupled due to the presence of permanent constraints triggering non-isotropic segmental motions[16]. This fraction of non-coupled network defects shows a significant dependence on cross-link density and on temperature similar to stress relaxation experiments[20]. Hence, selection of the temperature for these experiments is a key parameter and also for the Rouse relaxation time of the longest chains between topological restrictions, which roughly corresponds to the entanglement length at low crosslink density, since it is of the same order as that shown by the segmental relaxation time, which in turn is related to T_g[20]. Thus, temperature range for these measurements must be performed far above T_g to allow dynamics being sufficient to complete segmental averaging over all possible chain conformations on the time scale of the NMR experiment. In this way, the proper order parameter from the plateau range, which is proportional to cross-link density, could be achieved.

Assignment of the glass transition for PE has been, however, a matter of continued intensive study as well as widespread disagreement[47]. On one hand, some authors, based on experiments of ^{13}C Nuclear Magnetic Resonance, concluded that the β relaxation process could not be identified with the glass transition in either branched or linear polyethylene[48]. On the other hand, the relative lack of sensitivity to morphological factors (presence or absence of crystalline fraction) and the magnitude of the activation parameters have suggested that the γ relaxation has its origin in relatively localized molecular motions[49]. Thus, T_g of the amorphous phase for both PEs, LDPE and HDPE, will be considered of being located within the interval ranging from -130 ° to -100 ºC in this work[50].

Other important aspect to take into account in semicrystalline polymers is that the choice of temperature interval must be sufficient to avoid effect of crystals in the measurements. As deduced from the DSC results represented in Figure 2, temperatures above 140 ºC for the two types of PE would be suitable since both polymers are in an isotropic amorphous state. In addition, MSE results (see Figure 5a and 6a) confirm this result, where only soft phase are shown at 140 ºC. Furthermore, temperature interval

must not be extremely elevated with respect of the T_m to avoid the beginning of degradation[11].

The usual procedure for these experiments is based on the application of an improved Baum and Pines pulse sequence[16]. As a result, two experimental signals are obtained: reference **(**I_{ref}) and DQ intensities (I_{DQ}) as a function of the DQ evolution time, τ_{DQ}. In order to analyze the network structure of polymeric samples, the raw experimental data need to be normalized in such a way that the temperature-independent network structure effect can be separated from the temperature-dependent segmental dynamics. The sum of the two components ($I_{DQ} + I_{ref}$) provides the full magnetization of the sample, which includes signals from segments between constrains or dipolar coupled networks segments and uncoupled isotropic mobile protons. As coupled network segments typically relax faster than non-coupled protons, the identification of both contributions is quite easy. Following the data analysis procedure explained elsewhere[16], the contributions of the isotropically mobile parts is calculated using the following fitting function:

$$I_{ref} - I_{DQ} = A \times e^{-\left(\frac{\tau_{DQ}}{T_2}\right)} \quad (3)$$

where A is the fraction of sample with this behavior and T_2 is the transverse relaxation time. This sample fraction is related to polymer network defects (A), which is mainly composed by the sol fraction of extractable polymer chain segments and non-extractable dangling chain ends from the polymer network because of the recycle delay time applied in these experiments. The subtraction of the polymeric network defects allows discriminating information coming from the constraints to the movement of the chains (*i.e.*, cross-links and entanglements)[15] and quantifying the corresponding residual dipolar coupling distributions according a numerical inversion procedure explained elsewhere[51].

Hence, it is possible to measure the effect relies on the orientation dependence of the (fluctuating) dipolar coupling tensor with respect to the magnetic field which can be described by an orientation autocorrelation function (OACF) of the chain segments[18,52]. At short times, fast segmental dynamics occur in the range of nanoseconds to microseconds and the OACF of the polymer segments decays quickly, due to the fast local fluctuations between the accessible spatial conformations, until a plateau value is reached in the case of polymer network, independently of the nature of cross-

links[14,19,20]. In that region the measurable weak residual dipolar coupling D_{res} is directly proportional to a local dynamic order parameter of the polymer backbone, S_b, giving information about the network structure[16]:

$$S_b = k\frac{D_{res}}{D_{stat}} = \frac{3}{5} \times \frac{r^2}{N} \quad (4)$$

where k is a parameter that represents the local coupling topology and intra-segmental motions. This parameter should be used to rescale the static coupling constant, D_{stat}, determined by the fixed proton-proton distances, in order to account for averaging effects that occur on the level below the segmental (Kuhn) length. The term r^2 is referred to the ratio of the end-to-end vector to its average unperturbed melt state and N represents the number of statistical (Kuhn) segments between constraints.

Two different contributions of the isotropically mobile parts are observed into these samples, and for this reason, two types of "*defects*" are calculated as A_1 and A_2 according to the following equation:

$$I_{ref} - I_{DQ} = A_1 \times e^{-\left(\frac{\tau_{DQ}}{T_2}\right)} + A_2 \times e^{-\left(\frac{\tau_{DQ}}{T_2'}\right)} \quad (5)$$

where A_1 is the fraction of defects with T_2 as the transverse relaxation time, A_2 is the other fraction of defects with T_2' as the transverse relaxation time. Finally, A is the sum of A_1 and A_2, *i.e.*, the total amount of defects. Hence, Table 3 shows the values obtained for A_1, A_2 and A, together with those attained for T_2 and T_2'. An amount of around 34% of irradiated LDPE chains are coupled while the rest are elastically inactive (66% in LDPE_109 and 67% in LDPE_221). This latest fraction is mainly composed by the sol fraction of extractable polymer chain segments and non-extractable dangling chain ends from the polymer network. Accordingly, values for LDPE are higher than those exhibited by HDPE since in the former the insoluble content is inferior. In irradiated LDPE, an almost constancy of this fraction is noted with dose while a clear decrease is observed in HDPE due to the increase of PE incorporated into the network, as the dose is raised.

Table 3.Values of A_1, T_2, A_2, T_2' and A at 150ºC derived from equation 5.

Sample	***EB dose (kGy)***	***A_1 (%)***	***A_2 (%)***	**A (A_1+ A_2) (%)**	***T_2 (ms)***	***T_2' (ms)***	r^2
LDPE	0	35	39	74	37	4	0.998
LDPE_109	109	26	40	66	47	5	0.999
LDPE_221	221	28	39	67	66	5	0.999
HDPE	0	13	47	61	35	3	0.999
HDPE_67	67	23	29	52	64	6	0.999
HDPE_133	133	22	25	48	68	6	0.998
HDPE_233	233	16	27	43	54	5	0.999

A possible explanation for the results achieved from irradiated LDPE could be given, taking into account the following facts. On one hand, overall LDPE crystallinity is lower than that in HDPE at room temperature (temperature at which EB irradiation took place). Accordingly, a superior amorphous content is developed in LDPE, being the amorphous regions those where EB irradiation exerts, initially, more effects. On the other hand, LDPE contains more tertiary carbons than HDPE, whose involve less energy than primary or secondary carbons. Therefore, free radicals appear more easily and in a larger extent in LDPE because its molecular structure contains a higher amount of tertiary bonds with lower energy and because its amorphous fraction is greater. These radicals can undergo recombination leading to either crosslinks or chain branching in addition to scission of chains and oxidation reactions by incorporation of distinct oxidative species, among others. The sum for isotropically mobile parts (elastically inactive fraction) is around 66% for LDPE, as indicate the A values reported in Table 3, and this fraction is mainly composed by sol fraction of extractable polymer chain segments and non-extractable dangling chain ends from the polymer network. Thus, only around the 34% of the whole LDPE chains are involved in the polymer network. Hence, results from DQ NMR might indicate that the crosslinking is not the main process at 150ºC in the case of LDPE, because only around 34% of the whole chains are coupled.

In contrast, the fraction elastically inactive decreases as irradiation dose increases for HDPE at 150 ºC (see Table 3). The HDPE under study has been produced using a metallocene catalyst during polymerization, instead of performing its synthesis through more conventional Ziegler-Natta catalysts. Thus, the resultant HDPE has a

narrow molecular weight distribution[39], which promotes the crosslinking process once free radicals have been developed after EB irradiation, so the fraction elastically inactive in HDPE is lower than in LDPE at the same temperature. However, the fraction elastically inactive at the highest irradiation dose is analogous to that found in non-irradiated HDPE sample at 180 °C (see Figure 7). This fact may be ascribed to the slight rise of number of entanglements at that high temperature, compensating the non-existence of chemical crosslinks, in the non-irradiated HDPE.

Nevertheless, proportion of chains elastically active increases in the LDPE as temperature reaches 180ºC, as shown in Figure 7. This fact could be explained because additional cross-links may have occurred at that high temperature or the amount of entanglements might be increased, which seems less probable because the disentangled chain end fragments decreases as the temperature increases, in polymer melts[53].

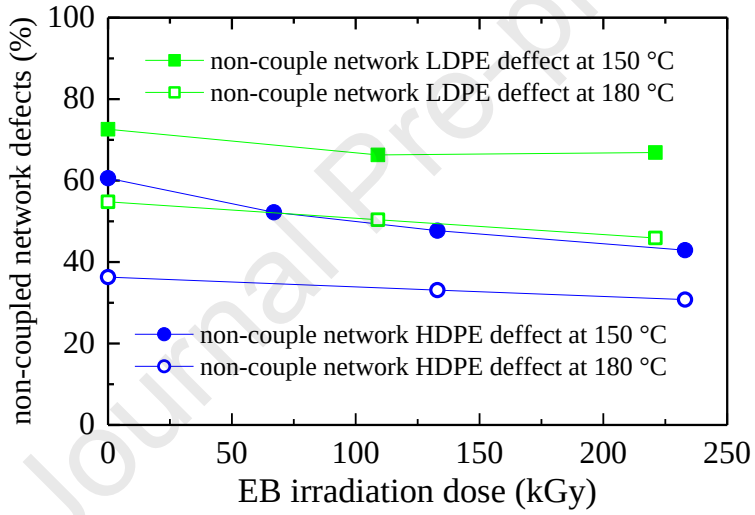

Figure 7. Variation of non-coupled network defects (A) as a function of EB irradiation for LDPE and HDPE at 150 ° and 180 °C.

Formation of cross-links (independent of their nature) renders non-isotropic the polymer segmental motion, whereby the chain segments become ordered with respect to the end-to-end distance, and residual dipolar couplings arise. According to this basic principle, the increase in D_{res} is directly related to the inverse of length of the chains between the constraints[54]. Hence, decrease in the number of defects is correlated with an increase in D_{res}, which is proportional to the network chain order parameter, as stated in equation 4 and observed in Figure 8a. Hence, D_{res} of non-irradiated specimens is due to entanglements between polymeric chains, the only constraint of polymer segmental motion possible in the molten state. Because of the different molecular architectures of

these two PEs, HDPE shows lower D_{res} than LDPE, which is a more branched polymer. D_{res} value increases as irradiation dose does in HDPE while this rise with EB dose is only slight for LDPE. Determination of the actual spatial distribution function of crosslink density is possible using the numerical inversion procedures, explained elsewhere[54,55], without any assumption about its shape.

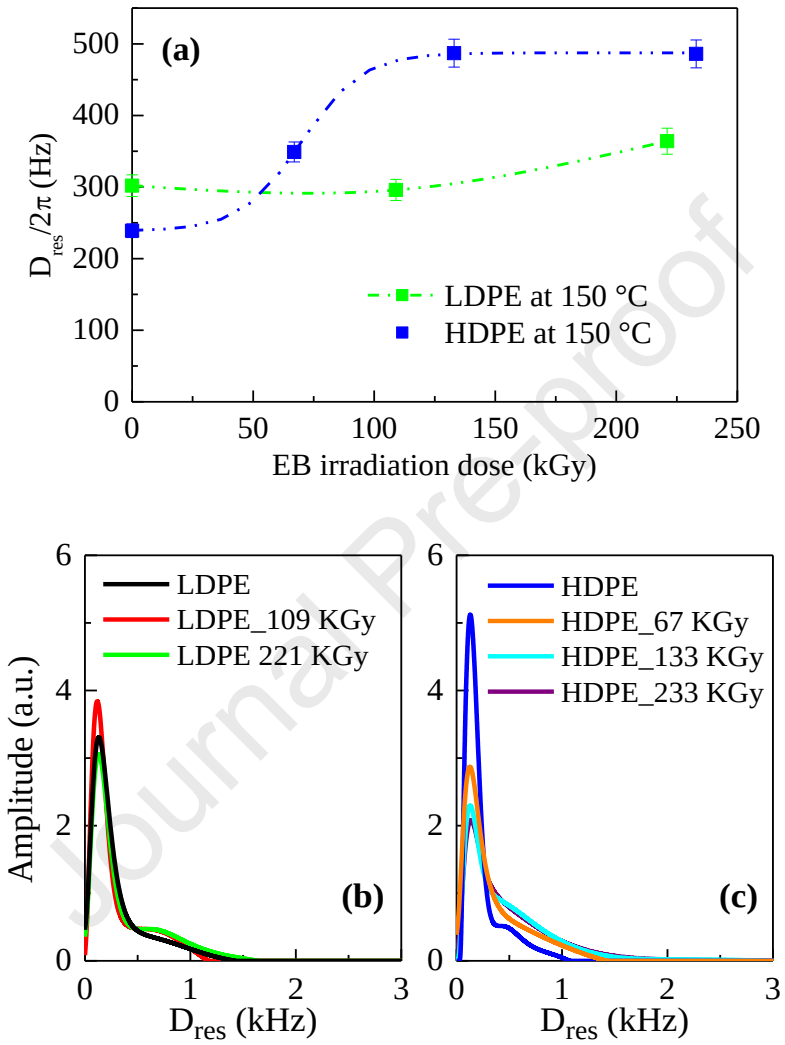

Figure 8. (a) Variation of the average residual dipolar couplings estimated from DQ experiments as a function of the EB irradiation dose at 150 °C. (b) Effect of irradiation dose on the distribution of the average residual dipolar couplings of LDPE at 150 °C (c) Effect of irradiation dose on the distribution of the average residual dipolar couplings of HDPE at 150 °C.

Figure 8b shows cross-link density distributions for the two PEs. Each specimen shows a single very broad crosslink density distribution with a tail at high M_c. Therefore, non-irradiated HDPE depicts a narrow entanglement distribution, which is consequence of its narrow molecular weight distributions. Instead, LDPE shows a broad entanglement distribution since its macrochains exhibit a broad molecular weight

distribution with great amount of branches. Therefore, only slightly variations for LDPE are observed in the crosslink density distribution as irradiation dose is enlarged, while HDPE shows an increase at high M_c as irradiation dose is raised. These results are in agreement with the decrease in the number of defects observed in HDPE. Taking into account the differences between the non-irradiated HDPE and LDPE specimens analyzed in this work, the distribution of crosslinks in the polymer is narrowed in the case of HDPE, while LDPE exhibits a broader distribution due to the great amount of branches in this polymeric matrix (see Figures 8b and 8c).

Finally, in order to confirm the results obtained in these PEs, a sample of isotactic polypropylene (iPP), non-irradiated and irradiated at 235 kGy, has been analyzed at the same temperature. In iPP, changes of the molar mass and formation of chain branching are the two main effects described by the action of EB irradiation[6,56]. Then, Figure 9 shows the normalized intensity for the DQ signals of the sequence pulse timing in non-irradiated and irradiated LDPE, HDPE and iPP at 150ºC.

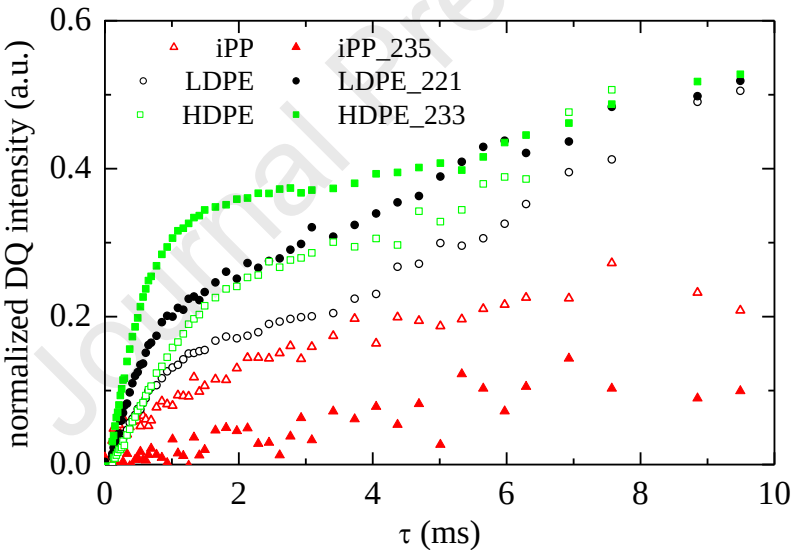

Figure 9.Normalized DQ-NMR intensity for LDPE, HDPE and PP at 150ºC.

On the basis of the data processing procedure described below, the elastically active network chains are distinguished and characterized. This fraction contributes to I_{DQ}, in contrast network defects, sol and solvent contributes to I_{ref}, in particular at long times. I_{DQ} is dominated by spin-pair DQ coherences[13,21,57] and comprises the structural information of the polymeric chains (the residual dipolar coupling constant D_{res} and its distribution), I_{ref} contains signal from half of the quantum orders ($4n$) of the dipolar coupled network chains, as well as the signal from uncoupled components (isotropically

mobile network defects like dangling chains and loops)[13]. The structural information in the polymeric network is separated from the relaxation effects due to chain dynamics by a point-by-point division of the DQ build up through the sum of the corrected relaxation function, where the contribution of defects are subtracted using equation 5. Hence, the obtained normalized DQ build up I_{nDQ} is then independent of relaxation effects and has to reach a long-time plateau value of 0.5, since I_{DQ} contains only half of the excited quantum orders ($4n$+2), according to DQ-NMR method[13,57].

$$I_{nDQ} = \frac{I_{DQ}}{I_{DQ} + I_{ref} - defects} \tag{6}$$

Results achieved show that PEs, either LDPE or HDPE, reach the plateau at 0.5, while that value is not achieved by the irradiated iPP, as shown in Figure 9.

Conclusions

Effect of irradiation dose and temperature was analyzed in two polyethylenes with different molecular architectures, LDPE and HDPE, by means of determination of gel content, DSC measurements and low-field solid state experiments by combination of two approaches: component analysis of MSE-refocused free-induction decays and DQ NMR experiments.

Gel content in non-irradiated specimens, independently of being LDPE or HDPE, was not detectable. Formation of a gel fraction and an increase in its amount was noticeable as irradiation dose rises, being this content in HDPE higher than in LDPE. Accordingly, a maximum value of 80 % in the former and of 60 % in the latest was reached at the highest dose applied, respectively.

Molecular differences existing in their respective macrochains were also evident in the location of their phase transitions, melting and crystallization, as well as the degree of crystallinity and amount in amorphous phase, as deduced from DSC results.

Phase composition and their evolution with the temperature were characterized by MSE-refocused free-induction measurements. Rigid fractions in LDPE and HDPE undergo a continuous decrease with increasing temperatures up to 100 and 120 °C, respectively, where an abrupt drop was observed associated with the main melting process occurring in these two PEs. This important reduction is opposite to the significant increase seen in the corresponding content in soft phase as isotropic melt is generated. Relaxation times (T_2^r) are one order of magnitude smaller in the rigid fractions of both PEs than in their respective soft phases, changing from few

microseconds for the former to hundreds of microseconds for the latest. Among these two phases, there is a fraction of polymer that exhibits a mobility gradient, called interphase. Hence, the relaxation time of this phase T_2^{sr} is intermediate between the ones found in the rigid and the soft phases. This three phase model shows a better agreement with the crystallinity degree estimated by DSC compared with the results found using a two-phase model.

DQ NMR measurements showed at 150 ºC that around 34% of irradiated chains in LDPE were coupled, indicating that the main process occurred by EB irradiation was not formation of crosslinks but chain scissions and chain branching, leading to a change in its molecular structure. As temperature increases, crosslinking rises in relation to other processes. In the HDPE, synthesized with a metallocene catalyst, elastically inactive fraction is lower than in LDPE at a given temperature because EB irradiation led to formation of crosslisking, which was boosted by its narrow molecular weight distribution.

Value of D_{res} was found inferior in the non-irradiated HDPE than in the LDPE with more branched chains, meaning a more broad entanglement distribution in the latest. Accordingly, the actual spatial cross-link density distribution was in HDPE narrower than in LDPE, in spite of both PEs showed a single and broad cross-link density distribution with a tail at high M_c. Effect of irradiation increased the crosslink density in HDPE, although dependence on dose was not significant. These results were in agreement with the decrease in number of defects observed in this polyethylene.

Comparison of results found in the two PEs with those achieved in an isotactic polypropylene allowed concluding that a network structure was created in both polyethylenes, although electron beam irradiation provokes differences with temperature and dose because of their intrinsic molecular characteristics.

Acknowledgments

Funding received from the 2017 Industrial Doctorate Program of the University of Cantabria, Spain, is gratefully acknowledged. Grants PID2020-119047RB-I00 and PID2020-114930GB-I00 were funded by MCIN/AEI/10.13039/501100011033.

References

(1) Ratner, B. D.; Hoffman, A. S.; Schoen, F. J.; Lemons, J. E. *Biomaterials Science: An Introduction to Materials in Medicine*; 2004.

(2) Cerrada, M. L.; Benavente, R.; Fernández-García, M.; Pérez, E.; Campos, J. M.; Ribeiro, M. R. Crosslinking in Metallocene Ethylene-Co-5,7-Dimethylocta-1,6-

Diene Copolymers Initiated by Electron-Beam Irradiation. *Polymer (Guildf).* **2009**, *50* (5), 1095–1102. https://doi.org/10.1016/j.polymer.2009.01.006.

(3) *Atomic Radiation and Polymers*; 1960. https://doi.org/10.1016/c2013-0-07861-9.

(4) Chodák, I. Properties of Crosslinked Polyolefin-Based Materials. *Prog. Polym. Sci.* **1995**, *20* (6), 1165–1199. https://doi.org/10.1016/0079-6700(95)98859-N.

(5) Lazár, M.; Rado, R.; Rychlý, J. Crosslinking of Polyolefins. *Adv. Polym. Sci.* **1990**, *95*, 148–197. https://doi.org/10.1007/3-540-52159-3_8.

(6) Cerrada, M. L.; Pérez, E.; Benavente, R.; Ressia, J.; Sarmoria, C.; Vallés, E. M. Gamma Polymorph and Branching Formation as Inductors of Resistance to Electron Beam Irradiation in Metallocene Isotactic Polypropylene. *Polym. Degrad. Stab.* **2010**, *95* (4), 462–469. https://doi.org/10.1016/j.polymdegradstab.2010.01.013.

(7) Valenza, A.; Piccarolo, S.; Spadaro, G. Influence of Morphology and Chemical Structure on the Inverse Response of Polypropylene to Gamma Radiation under Vacuum. *Polymer (Guildf).* **1999**, *40* (4), 835–841. https://doi.org/10.1016/s0032-3861(98)00294-8.

(8) Tobita, H.; Kawai, H. Simulation of Size Exclusion Chromatography for Branched Polymers Formed by Simultaneous Long-Chain Branching and Random Scission. *E-Polymers* **2002**, *2* (1), 1–13. https://doi.org/10.1515/epoly.2002.2.1.688.

(9) Cerrada, María L.;Rodriguez-Amor, V;Perez, E. Effects of Clay Nanoparticles and Electron Irradiation in the Crystallization Rate of Syndiotactic Polypropylene. *J. Polym. Sci. Part B Polym. Phys.* **2007**, *45*, 1068–1076.

(10) Cota, S. S.; Vasconcelos, V.; Senne, M.; Carvalho, L. L.; Rezende, D. B.; Correa, R. F. Changes in Mechanical Properties Due to Gamma Irradiation of High-Density Polyethylene (HDPE). *Brazilian J. Chem. Eng.* **2007**, *24* (2), 259–265. https://doi.org/10.1590/S0104-66322007000200010.

(11) Hedesiu, C.; Demco, D. E.; Kleppinger, R.; Buda, A. A.; Blümich, B.; Remerie, K.; Litvinov, V. M. The Effect of Temperature and Annealing on the Phase Composition, Molecular Mobility and the Thickness of Domains in High-Density Polyethylene. *Polymer (Guildf).* **2007**, *48* (3), 763–777. https://doi.org/10.1016/j.polymer.2006.12.019.

(12) Campise, F.; Agudelo, D. C.; Acosta, R. H.; Villar, M. A.; Vallés, E. M.; Monti, G. A.; Vega, D. A. Contribution of Entanglements to Polymer Network

Elasticity. *Macromolecules* **2017**, *50* (7), 2964–2972. https://doi.org/10.1021/acs.macromol.6b02784.

(13) Chassé, W.; Lang, M.; Sommer, J. U.; Saalwächter, K. Cross-Link Density Estimation of PDMS Networks with Precise Consideration of Networks Defects. *Macromolecules* **2012**, *45* (2), 899–912. https://doi.org/10.1021/ma202030z.

(14) Che, J.; Toki, S.; Valentin, J. L.; Brasero, J.; Nimpaiboon, A.; Rong, L.; Hsiao, B. S. Chain Dynamics and Strain-Induced Crystallization of Pre- and Postvulcanized Natural Rubber Latex Using Proton Multiple Quantum NMR and Uniaxial Deformation by in Situ Synchrotron X-Ray Diffraction. *Macromolecules* **2012**, *45* (16), 6491–6503. https://doi.org/10.1021/ma3006894.

(15) Malmierca, M. A.; González-Jiménez, A.; Mora-Barrantes, I.; Posadas, P.; Rodríguez, A.; Ibarra, L.; Nogales, A.; Saalwächter, K.; Valentín, J. L. Characterization of Network Structure and Chain Dynamics of Elastomeric Ionomers by Means of 1H Low-Field NMR. *Macromolecules* **2014**, *47* (16), 5655–5667. https://doi.org/10.1021/ma501208g.

(16) Saalwächter, K. Proton Multiple-Quantum NMR for the Study of Chain Dynamics and Structural Constraints in Polymeric Soft Materials. *Prog. Nucl. Magn. Reson. Spectrosc.* **2007**, *51* (1), 1–35. https://doi.org/10.1016/j.pnmrs.2007.01.001.

(17) Saalwächter, K. Detection of Heterogeneities in Dry and Swollen Polymer Networks by Proton Low-Field NMR Spectroscopy. *J. Am. Chem. Soc.* **2003**, *125* (48), 14684–14685. https://doi.org/10.1021/ja038278p.

(18) Vaca Chávez, F.; Saalwächter, K. Time-Domain NMR Observation of Entangled Polymer Dynamics: Universal Behavior of Flexible Homopolymers and Applicability of the Tube Model. *Macromolecules* **2011**, *44* (6), 1549–1559. https://doi.org/10.1021/ma1025708.

(19) Valentín, J. L.; López, D.; Hernández, R.; Mijangos, C.; Saalwächter, K. Structure of Polyvinyl Alcohol Cryo-Hydrogels as Studied by Proton Low-Field NMR Spectroscopy. *Macromolecules* **2009**, *42* (1), 263–272. https://doi.org/10.1021/ma802172g.

(20) Valentín, J. L.; Posadas, P.; Fernández-Torres, A.; Malmierca, M. A.; González, L.; Chassé, W.; Saalwächter, K. Inhomogeneities and Chain Dynamics in Diene Rubbers Vulcanized with Different Cure Systems. *Macromolecules* **2010**, *43* (9), 4210–4222. https://doi.org/10.1021/ma1003437.

(21) Graf, R.; Demco, D. E.; Hafner, S.; Spiess, H. W. Selective Residual Dipolar Couplings in Cross-Linked Elastomers by 1H Double-Quantum NMR Spectroscopy. *Solid State Nucl. Magn. Reson.* **1998**, *12* (2–3), 139–152. https://doi.org/10.1016/S0926-2040(98)00058-7.

(22) Maus, A.; Hertlein, C.; Saalwächter, K. A Robust Proton NMR Method to Investigate Hard/Soft Ratios, Crystallinity, and Component Mobility in Polymers. *Macromol. Chem. Phys.* **2006**, *207* (13), 1150–1158. https://doi.org/10.1002/macp.200600169.

(23) Quinn, F. A.; Mandelkern, L. Thermodynamics of Crystallization in High Polymers: Poly-(Ethylene). *J. Am. Chem. Soc.* **1958**, *80* (13), 3178–3182. https://doi.org/10.1021/ja01546a003.

(24) Wunderlich, B. *Macromolecular Physics, Vol 3*, Macromolec.; Press, A., Ed.; New York, 1980.

(25) Arranz-Andrés, J.; Parrilla, R.; Cerrada, M. L.; Pérez, E. Mesophase Formation in Random Propylene-Co-1-Octene Copolymersss. *Macromolecules* **2013**, *46* (21), 8557–8568. https://doi.org/10.1021/ma401539u.

(26) Pérez, E.; Cerrada, M. L.; Benavente, R.; Gómez-Elvira, J. M. Enhancing the Formation of the New Trigonal Polymorph in Isotactic Propene-1-Pentene Copolymers: Determination of the X-Ray Crystallinity. *Macromol. Res.* **2011**, *19* (11), 1179–1185. https://doi.org/10.1007/s13233-011-1103-6.

(27) Marek, A. A.; Verney, V. Rheological Behavior of Polyolefins during UV Irradiation at High Temperature as a Coupled Degradative Process. *Eur. Polym. J.* **2015**, *72*, 1–11. https://doi.org/10.1016/j.eurpolymj.2015.09.003.

(28) Satti, A. J.; Andreucetti, N. A.; Vallés, E. M.; Carella, J. M.; Pérez, C. J. Use of SSA to Detect Structural Changes in Metallocenic Ethylene/α-Olefin Copolymers and Their Free Radical Post-Reactor Modifications. *Polym. Degrad. Stab.* **2016**, *125*, 43–48. https://doi.org/10.1016/j.polymdegradstab.2016.01.001.

(29) Cerrada, M. L.; Benavente, R.; Fernández-García, M.; Pérez, E.; Campos, J. M.; Ribeiro, R. Metallocene Ethylene-Co-(5,7-Dimethylocta-1, 6-Diene) Copolymers Crosslinked Using Electron Beam Irradiation: A Tunable Alternative. *Polym. Int.* **2011**, *60* (9), 1309–1317. https://doi.org/10.1002/pi.3082.

(30) Eckman, R. R.; Henrichs, P. M.; Peacock, A. J. Study of Polyethylene by Solid State NMR Relaxation and Spin Diffusion. *Macromolecules* **1997**, *30* (8), 2474–2481. https://doi.org/10.1021/ma9516753.

(31) Shirayama, K.; Kita, S.-I.; Watabe, H. Effects of Branching on Some Properties of Ethylene/A-olefin Copolymers. *Die Makromol. Chemie* **1972**, *151* (1), 97–120. https://doi.org/10.1002/macp.1972.021510108.

(32) Alamo, R. G.; Viers, B. D.; Mandelkern, L. Phase Structure of Random Ethylene Copolymers: A Study of Counit Content and Molecular Weight as Independent Variables. *Macromolecules* **1993**, *26* (21), 5740–5747. https://doi.org/10.1021/ma00073a031.

(33) Alamo, R.; Domszy, R.; Mandelkern, L. Thermodynamic and Structural Properties of Copolymers of Ethylene. *J. Phys. Chem.* **1984**, *88* (26), 6587–6595. https://doi.org/10.1021/j150670a022.

(34) Mcfaddin, D. C.; Russell, K. E.; Wu, G.; Heyding, R. D. Characterization of Polyethylenes by X-ray Diffraction and 13C-NMR: Temperature Studies and the Nature of the Amorphous Halo. *J. Polym. Sci. Part B Polym. Phys.* **1993**, *31* (2), 175–183. https://doi.org/10.1002/polb.1993.090310206.

(35) Pérez, E.; Bello, A.; Pereña, J. M.; Benavente, R.; Martínez, M. C.; Aguilar, C. Solid-State Nuclear Magnetic Resonance Study of Linear Low-Density Polyethylenes: 1. Ethylene-1-Butene Copolymers. *Polymer (Guildf).* **1989**, *30* (8), 1508–1512. https://doi.org/10.1016/0032-3861(89)90224-3.

(36) Minick, J. Moet, A., Hiltner, A., Baer, E. and Chum, S. P. Crystallization of Very l o w Density Copolymers of Ethylene with A-Olefins. *J Appl Polym Sci.* **1995**, *58*, 1371–1384.

(37) Pérez, E.; VanderHart, D. L.; Crist, B.; Howard, P. R. Morphological Partitioning of Ethyl Branches in Polyethylene By13C Nuclear Magnetic Resonance. *Macromolecules* **1987**, *20* (1), 78–87. https://doi.org/10.1021/ma00167a015.

(38) VanderHart, D. L.; Pérez, E. A 13C NMR Method for Determining the Partitioning of End Groups and Side Branches between the Crystalline and Noncrystalline Regions in Polyethylene. *Macromolecules* **1986**, *19* (7), 1902–1909. https://doi.org/10.1021/ma00161a020.

(39) Cerrada, M. L.; Benavente, R.; Pérez, E.; Moniz-Santos, J.; Ribeiro, M. R. Metallocenic Copolymers of Ethylene and 5,7-Dimethylocta-1,6-Diene: Structural Characterization and Mechanical Behavior. *J. Polym. Sci. Part B Polym. Phys.* **2004**, *42* (20), 3797–3808. https://doi.org/10.1002/polb.20248.

(40) Blümich, B.; Casanova, F.; Buda, A.; Kremer, K.; Wegener, T. Mobile NMR for Analysis of Polyethylene Pipes. In *Acta Physica Polonica A*; Polish Academy of

Sciences, 2005; Vol. 108, pp 13–23. https://doi.org/10.12693/APhysPolA.108.13.

(41) Mauri, M.; Thomann, Y.; Schneider, H.; Saalwächter, K. Spin-Diffusion NMR at Low Field for the Study of Multiphase Solids. *Solid State Nucl. Magn. Reson.* **2008**, *34* (1–2), 125–141. https://doi.org/10.1016/j.ssnmr.2008.07.001.

(42) Meyer, H. W.; Schneider, H.; Saalwächter, K. Proton NMR Spin-Diffusion Studies of PS-PB Block Copolymers at Low Field: Two- vs Three-Phase Model and Recalibration of Spin-Diffusion Coefficients. *Polym. J.* **2012**, *44* (8), 748–756. https://doi.org/10.1038/pj.2012.88.

(43) Pérez, E.; Benavente, R.; Quijada, R.; Narváez, A.; Barrera Galland, G. Structure Characterization of Copolymers of Ethylene and 1-Octadecene. *J. Polym. Sci. Part B Polym. Phys.* **2000**, *38* (11), 1440–1448. https://doi.org/10.1002/(SICI)1099-0488(20000601)38:11<1440::AID-POLB40>3.0.CO;2-O.

(44) Begmann, K. Study of the Molecular Motions of Polyethylene By Line-Shape Analysis of Broad-Line Proton Nmr Spectra. *J Polym Sci Polym Phys Ed* **1978**, *16* (9), 1611–1634. https://doi.org/10.1002/pol.1978.180160907.

(45) Hansen, E. W.; Kristiansen, P. E.; Pedersen, B. Crystallinity of Polyethylene Derived from Solid-State Proton NMR Free Induction Decay. *J. Phys. Chem. B* **1998**, *102* (28), 5444–5450. https://doi.org/10.1021/jp981753z.

(46) Angel Jose´Satti, 1, 2Noemı´Amalia Andreucetti, 1Rau´l Quijada, 3Claudia Sarmoria, 2Jose´Marı´a Pastor, 4Enrique Marcelo Valle´s. Gamma-Irradiated Metallocenic Polyethylene AndEthylene-1-Hexene Copolymers. *J. Appl. Polym. Sci.* **2010**, *117* (1), 290–301. https://doi.org/10.1002/app.

(47) Âa, M.; Cerrada, L.; Benavente, R.; Pe Ârez, E.; Moniz-Santos, J.; Ribeiro, M. R. *Experimental Evidence of the Glass Transition in a Metallocene Ethylene-1-Octene Copolymer and Its Composites with Glass ®bre*.

(48) Dechter, J. J.; Axelson, D. E.; Dekmezian, A.; Glotin, M.; Mandelkern, L. ANALYSIS OF THE Beta TRANSITION OF LINEAR AND BRANCHED POLYETHYLENES BY CARBON-13 NMR. *J. Polym. Sci. Part A-2, Polym. Phys.* **1982**, *20* (4), 641–650. https://doi.org/10.1002/pol.1982.180200407.

(49) Boyd, R. H. Linear Polyethylenet G * -Gr. **1984**, 903–911.

(50) Geil, P. H. Polymer Characterization. *Mod. Text. Charact. Methods* **2017**, No. 800, 9–143. https://doi.org/10.1201/9780203746684.

(51) Sommer, J. U.; Saalwächter, K. Segmental Order Parameters and Swelling in

Polymer Networks. *Macromol. Symp.* **2010**, *291–292* (1), 251–257. https://doi.org/10.1002/masy.201050529.

(52) Vaca Chávez, F.; Saalwächter, K. NMR Observation of Entangled Polymer Dynamics: Tube Model Predictions and Constraint Release. *Phys. Rev. Lett.* **2010**, *104* (19), 1–4. https://doi.org/10.1103/PhysRevLett.104.198305.

(53) Litvinov, V. M.; Ries, M. E.; Baughman, T. W.; Henke, A.; Matloka, P. P. Chain Entanglements in Polyethylene Melts. Why Is It Studied Again? *Macromolecules* **2013**, *46* (2), 541–547. https://doi.org/10.1021/ma302394j.

(54) Weese, J. A Regularization Method for Nonlinear Ill-Posed Problems. *Comput. Phys. Commun.* **1993**, *77* (3), 429–440. https://doi.org/10.1016/0010-4655(93)90187-H.

(55) Weese, J. A Reliable and Fast Method for the Solution of Fredhol Integral Equations of the First Kind Based on Tikhonov Regularization. *Comput. Phys. Commun.* **1992**, *69* (1), 99–111. https://doi.org/10.1016/0010-4655(92)90132-I.

(56) Auhl, D.; Stange, J.; Münstedt, H.; Krause, B.; Voigt, D.; Lederer, A.; Lappan, U.; Lunkwitz, K. Long-Chain Branched Polypropylenes by Electron Beam Irradiation and Their Rheological Properties. *Macromolecules* **2004**, *37* (25), 9465–9472. https://doi.org/10.1021/ma030579w.

(57) Saalwächter, K.; Ziegler, P.; Spyckerelle, O.; Haidar, B.; Vidal, A.; Sommer, J. U. 1H Multiple-Quantum Nuclear Magnetic Resonance Investigations of Molecular Order Distributions in Poly(Dimethylsiloxane) Networks: Evidence for a Linear Mixing Law in Bimodal Systems. *J. Chem. Phys.* **2003**, *119* (6), 3468–3482. https://doi.org/10.1063/1.1589000.

Highlights

- Initial PE architecture controls gel content developed through EB irradiation.
- Crosslinking increases with EB doses, being more noticeable in HDPE than in LDPE.
- Values from three phase model agree better with crystallinity estimated by DSC.
- Relaxation times are much smaller in the rigid than in the soft phases for both PEs.

Declaration of interests

☒ The authors declare that they have no known competing financial interests or personal relationships that could have appeared to influence the work reported in this paper.

☐ The authors declare the following financial interests/personal relationships which may be considered as potential competing interests: